Sparse Microwave Breast Imaging with Differently Polarized Arrays

Marija Nikolic Stevanovic, Jelena Dinkic, Jasmin Music
University of Belgrade,
School of Electrical Engineering
Belgrade, 11120 Serbia
mnikolic@etf.rs

Arye Nehorai
Preston M. Green ECE Department,
Washington University in St. Louis,
St. Louis, MO, USA
nehorai@wustl.edu

***Abstract*—We investigate the role of polarization in sparse differential microwave imaging for the breast-cancer localization. We consider two types of antenna arrays, placed around realistic inhomogeneous breast models. In the first case, the antennas are vertical with respect to the chest wall, whereas in the second case, the antennas are located in the horizontal planes, parallel to the chest wall. In the approximate linear model, we use numerically computed three-dimensional (3-D) Green's functions, assuming that the breast tissue parameters are known from the previous measurements. By introducing some deviation in the permittivity of the breast tissues, we compare the estimation accuracy yielded by different array configurations and assess the robustness of the sparse approach.**

Keywords—microwave imaging; sparse processing; breast cancer localization

I. INTRODUCTION

In the recent years, there has been a growing interest in microwave medical imaging [1]-[6]. Compared to conventional technologies, the main advantages of microwave imaging systems are their portability, low-cost, and non-ionizing radiation.

In this paper, we consider the application of sparse processing [7] for the breast-cancer localization. Compressive sensing or sparse imaging is known to yield clean and focused images with suppressed artifacts [8]. These techniques are particularly suitable in cases in which targets occupy only a fraction of the observed domain. Hence, there is a great perspective in applying the sparse processing in differential microwave imaging where the goal is to locate small changes in the breast tissue (i.e., lesions) that appeared between consecutive measurements.

In this framework, we investigate the utilization of two differently polarized arrays. In the first case, the antennas are vertically placed, as illustrated in Fig. 1(a). This measurement configuration is analogous to the transverse magnetic (TM) polarization in the two-dimensional geometry (2-D). In the second case, which is depicted in Fig. 1(b), the antennas are placed horizontally. This measurement configuration corresponds to the transverse electric (TE) polarization in 2-D geometry. In the considered models, we took the trans-polarization fully into account.

This work was supported by the AFOSR Grant No. FA9550-11-1-0210, and by the Serbian Ministry of Science and Education under the Grant TR32005. The work has been partially developed in the framework of COST Action TD1301 MiMed.

As a healthy breast model, we used a realistic 3-D breast phantom based on magnetic resonance imaging [9], [10]. We assumed that permittivity and conductivity distribution of the breast model are known up to some extent. We studied the influence of the array polarization to the algorithm robustness [11] against the tissue parameter errors.

II. MEASUREMENT MODEL

We consider a measurement scenario depicted in Fig. 1. An unknown target or lesion (illustrated as a green inclusion) is located inside a non-magnetic inhomogeneous breast tissue.

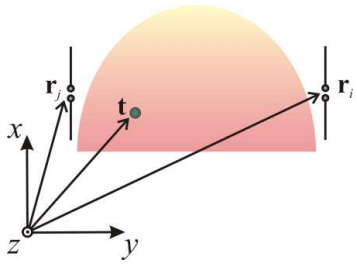

(a)

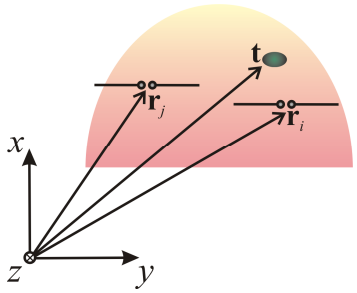

(b)

Fig. 1. Two measurement configurations and the adopted coordinate system: (a) quasi-TM polarization and (b) quasi-TE polarization.

978-0-9928-6265-7/16/$31.00 ©2016 IEEE

For determining the lesion location, we compare antenna arrays with different polarizations. Fig. 1(a) shows the first array consisting of the antennas parallel to the *x*-axis (quasi TM polarization). Fig. 1(b) shows the second array, in which the antennas are parallel to the *z*0*y* plane of the adopted coordinate system (quasi TE polarization).

We define the scattered field as

$$\mathbf{E}_{\mathrm{s}}(\mathbf{r}) = \mathbf{E}(\mathbf{r}) - \mathbf{E}_{\mathrm{b}}(\mathbf{r}), \tag{1}$$

where $\mathbf{r}$ denotes the field point, $\mathbf{E}$ is the electric field vector measured when the lesion is inside the breast, and $\mathbf{E}_{\mathrm{b}}$ is the electric field vector obtained for the healthy breast. The field scattered from an electrically small target is approximately [12]

$$\mathbf{E}_{\mathrm{s}}(\mathbf{r}) \approx \mathrm{j}\omega(\varepsilon - \varepsilon_{\mathrm{b}}(\mathbf{r}'))\overline{\mathbf{G}}_{\mathrm{b}}(\mathbf{r},\mathbf{r}')\mathbf{E}(\mathbf{r}')\Delta V, \tag{2}$$

where $\mathbf{r}'$ is the source position vector (coinciding with the lesion location), $\overline{\mathbf{G}}_{\mathrm{b}}(\mathbf{r},\mathbf{r}')$ is the Dyadic Green's function computed for the healthy breast, $\mathbf{E}(\mathbf{r}')$ is the total field inside the breast with the lesion, ε_{b} is the permittivity of the healthy breast, ε is the permittivity of the lesion $(\varepsilon \neq \varepsilon_{\mathrm{b}})$, and ΔV is the volume of the lesion. For weak scatterers, (2) becomes

$$\mathbf{E}_{\mathrm{s}}(\mathbf{r}) \approx \mathrm{j}\omega(\varepsilon - \varepsilon_{\mathrm{b}})\overline{\mathbf{G}}_{\mathrm{b}}(\mathbf{r},\mathbf{r}')\mathbf{E}_{\mathrm{b}}(\mathbf{r}')\Delta V, \tag{3}$$

where $\mathbf{E}_{\mathrm{b}}(\mathbf{r}')$ is the field inside the healthy breast (i.e., the background medium). Assuming that the antennas in the array are electrically short dipoles and that the *i*th antenna is transmitting, the field in the background medium is

$$\mathbf{E}_{\mathrm{b}}(\mathbf{r}') \approx I_0 \overline{\mathbf{G}}_{\mathrm{b}}(\mathbf{r}',\mathbf{r}_i)\cdot\mathbf{h}_i,\ \|\mathbf{h}_i\| = h,\ i = 1,\ldots,M, \tag{4}$$

where I_0 is the current at the antenna port; $\mathbf{r}_i$ is the location of the *i*th antenna; $\mathbf{h}_i$ is the vector parallel to the axis of the *i*th dipole and in the direction of the current; and M is the total number of the antennas in the array. The scattered field at the *j*th receiver is

$$\mathbf{E}_{\mathrm{s}}(\mathbf{r}_j) \approx \mathrm{j}\omega(\varepsilon - \varepsilon_{\mathrm{b}})\overline{\mathbf{G}}_{\mathrm{b}}(\mathbf{r}_j,\mathbf{r}')\overline{\mathbf{G}}_{\mathrm{b}}(\mathbf{r}',\mathbf{r}_i)\cdot\mathbf{h}_i I_0 \Delta V, \tag{5}$$

where $\mathbf{r}_j$ is the location of the *j*th antenna. Due to reciprocity, (5) becomes

$$\mathbf{E}_{\mathrm{s}}(\mathbf{r}_j) \approx \mathrm{j}\omega(\varepsilon - \varepsilon_{\mathrm{b}})\left(\overline{\mathbf{G}}_{\mathrm{b}}(\mathbf{r}',\mathbf{r}_j)\right)^{\mathrm{T}}\overline{\mathbf{G}}_{\mathrm{b}}(\mathbf{r}',\mathbf{r}_i)\cdot\mathbf{h}_i\, I_0 \Delta V, \tag{6}$$

Finally, the received signal is

$$\varepsilon(\mathbf{r}_j,\mathbf{r}_i) = -\mathbf{E}_{\mathrm{s}}\cdot\mathbf{h}_j,\ j = 1,\ldots,M, \tag{7}$$

where $\mathbf{h}_j$ is the vector in the direction of the current of the *j*th antenna and parallel to its axis.

III. SPARSE MODEL

We search for the target (lesion) on a uniform 3-D grid inside the breast volume. Assuming that there is a target at each node simultaneously, we derive a linear model

$$\mathbf{e}_i = \mathbf{G}_i^{x(yz)}\mathbf{c}, \tag{8}$$

$$\mathbf{e}_i = \left[\varepsilon(\mathbf{r}_1,\mathbf{r}_i)\ \ \ldots\ \ \varepsilon(\mathbf{r}_M,\mathbf{r}_i)\right]^{\mathrm{T}}, \tag{9}$$

$$\mathbf{c} = \left[c_1\ \ \ldots\ \ c_N\right]^{\mathrm{T}}, \tag{10}$$

where $\mathbf{e}_i$ is the vector of the received signals when the *i*th antenna is transmitting, $\mathbf{G}_i^{x}$ is the system matrix corresponding to the antennas parallel to the *x*-axis, $\mathbf{G}_i^{yz}$ is the system matrix corresponding to the antennas parallel to the *yz* plane, and $\mathbf{c}$ is the unknown vector whose elements are proportional to the contrast functions of the grid elements. In both cases, we assume that all antennas receive signals. We combine the measurement models (8)-(10) related to different transmitters into one set of equations

$$\mathbf{e} = \mathbf{G}^{x(yz)}\mathbf{c}, \tag{11}$$

where $\mathbf{e}$ is the stacked measurement vector, and $\mathbf{G}$ is the total system matrix $\mathbf{G}^{x(yz)}$. Since the target occupies only a few grid nodes, we apply the l_1 regularization to emphasize the significant elements of the solution vector $\mathbf{c}$

$$\hat{\mathbf{c}} = \min_{\mathbf{c}}\left\{\|\mathbf{e} - \mathbf{G}\mathbf{c}\|_2^2 + \lambda\|\mathbf{c}\|_1\right\}, \tag{12}$$

where $\hat{\mathbf{c}}$ is the estimated coefficient vector and λ is the regularization parameter. The first term on the right-hand side of (12) minimizes the error between the estimated model and the measurements, whereas the second term minimizes the number of the significant elements of the solution vector. The regularization parameter (λ), balances between those requirements. To compute the regularization parameter, we use the L-curve method [13].

IV. Breast Model

To compare differently polarized arrays, we used the inhomogeneous breast model (Breast ID: 012204) provided by the UWCEM Numerical Breast Phantom Repository [9]. We discretized a continuous range of the breast permittivity and conductivity values into seven homogeneous domains [14]. In the first two rows of the Table 1, we give the associated tissue parameters. Approximately, the domain #1 corresponds to the fatty region, the domains #2-4 belong to the transitional tissue, and the domains #5-7 correspond to the fibro-glandular tissue. Besides, the permittivity and the conductivity of the skin were $\varepsilon_r = 39$ and $\sigma = 0.9\,\text{S/m}$, respectively. By changing the properties of one voxel ($5\,\text{mm} \times 5\,\text{mm} \times 5\,\text{mm}$), we added the tumor in the model. The permittivity and the conductivity of the tumor were $\varepsilon_r = 56$ and $\sigma = 1\,\text{S/m}$, respectively.

In Fig. 2, we show the outer appearance of the breast phantom, along with the arrays corresponding to the quasi TM and TE polarization. Fig. 3 illustrates the position of the tumor inside the phantom.

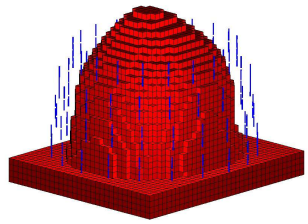

(a)

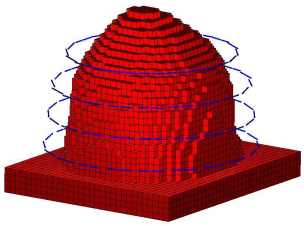

(b)

Fig. 2. Antenna arrays used in the numerical simulations: (a) quasi TM polarization or *x*-polarization and (b) qausi TE polarization or *yz* polarization.

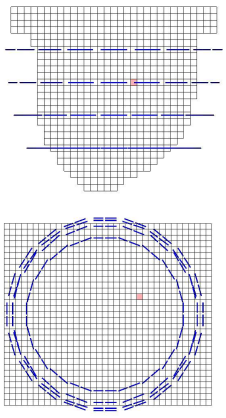

Fig. 3. Position of the lesion inside the breast illustrated for horizontally polarized antennas (quasi TE case).

TABLE I. Domain Permittivities

Domain	1	2	3	4	5	6	7
σ [S/m]	0.06	0.21	0.36	0.49	0.68	0.93	1.28
ε_r	5	15	24	32	42	51	60
ε_{r_err}	5.7	15.6	23	30.7	43.7	53	62.4

V. Numerical Model

The arrays consisted of 80 dipoles placed around the breast model. The operating frequency was $f = 1\,\text{GHz}$. The length of a dipole was $h = 2\,\text{cm}$. To compute the array response and the Dyadic Green's functions, we used the software WIPL-D Pro [15]. We corrupted the measurement data by adding white Gaussian noise. We defined the signal-to-noise ratio (*SNR*) with respect to the power of the scattered field.

As the benchmark, we considered the ideal case, in which the parameters of the tissues were exactly known. The size of the search grid was $N_x \times N_y \times N_z$, where $N_x = 10$, $N_y = 20$, $N_z = 20$. The algorithm searched for the target in all $N_x N_y N_z = 4000$ points simultaneously. In Fig. 4, we show the result in the true plane. The elements of the solution vector in all other planes were zero. Even for values of the *SNR* as low as *SNR* = 0 dB, the target was located correctly.

In the second case, the permittivities of all domains were altered for 4%. The permittivity values used in the simulations were given in the last row of the Table 1. Fig. 5 shows the result of the sparse algorithm when the antennas were parallel to the *x*-axis. The true target was located in the right position and plane. However, there was also a false target due to the ambiguities in the breast tissue parameters. In Fig. 6, we present the localization result related to the antennas parallel to the *yz* plane. The true target was located at the right place. However, the ghost targets appeared in other plane (Fig. 7). Hence, the position of the true target was the same in both cases. In contrast, the false targets were at different positions for the two arrays. Hence, using different polarizations may help in increasing the sensitivity of the algorithm and in eliminating the false targets.

VI. Conclusion

We considered the sparse processing framework for the breast cancer localization using microwave measurements obtained with differently polarized arrays. We showed that when the tissue parameters are not completely known, array versatility is important for improving the estimation accuracy and for distinguishing between true and false targets.

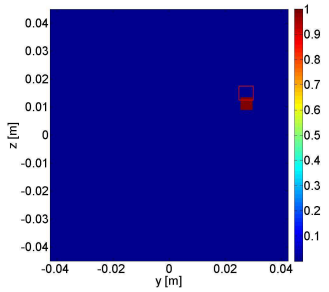

Fig. 4. Result of the localization in the case when the paraters of the breast were completely known. The true plane.

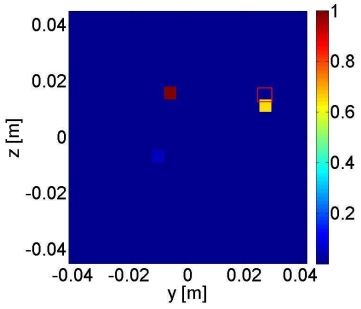

Fig. 5. Result of the localization in the case when the antennas are parallel to the *x*-axis and the breast tissue parameters are known with the 4% error. The targets were found in the true plane.

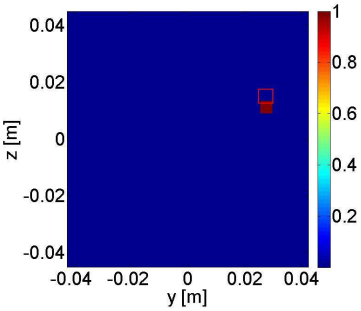

Fig. 6. Result of the localization in the case when the antennas are parallel to the *yz*-plane and the breast tissue parameters are known with the 4% error. The true plane.

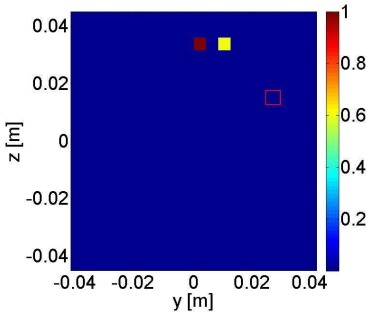

Fig. 7. Result of the localization in the case when the antennas are parallel to the *yz*-plane and the breast tissue parameters are known with the 4% error. The plane separated by 1 cm from the true plane.

REFERENCES

[1] S. Semenov, "Microwave tomography: Review of the progress towards clinical applications," *Phil. Trans. R. Soc. A*, vol. 367, pp. 3021–3042, 2009.

[2] A. M. Hassan, M. El-Shenawee, "Review of Electromagnetic Techniques for Breast Cancer Detection," IEEE Reviews in Biomedical Engineering, vol.4, no., pp.103-118, 2011.

[3] P. M. Meaney, M. W. Fanning, T. Raynolds, C. J. Fox, Q. Q. Fang, C. A. Kogel, S. P. Poplack, and K. D. Paulsen, "Initial clinical experience with microwave breast imaging in women with normal mammography," Acad. Radiol., vol. 14, no. 2, pp. 207–218, Feb. 2007.

[4] M. Klemm, J. Leendertz, A. W. Preece, M. Shere, I. J. Craddock, and R. Benjamin, "Clinical experience of breast cancer imaging using ultrawidebandmicrowave radar systemat Bristol," in *IEEE AP-S Int. Symp.*, Toronto, ON, Canada, 2010, vol. 501.10.

[5] P. M. Meaney, D. Goodwin, A. H. Golnabi, T. Zhou, M. Pallone, S. D. Geimer, G. Bruke, and K. D. Paulsen, "Clinical microwave tomographic imaging of the calcaneus: A first-in-human case study of two subjects," *IEEE Trans. Biomed. Eng.*, vol. 59, no. 12, pp. 3304–3313, Dec. 2012.

[6] I. S. Karanasiou, N. K. Uzunoglu, and C. C. Papageorgiou, "Towards functional noninvasive imaging of excitable tissues inside the human body using focused microwave radiometry," *IEEE Trans. Microw.Theory Techn.*, vol. 52, no. 8, pp. 1898–1908, Aug. 2004.

[7] D. M. Malioutov, M. Cetin, and A. S. Willsky, "Sparse signal reconstruction perspective for source localization with sensor arrays," IEEE Trans. Signal Process., vol. 53, no. 8, pp. 3010–3022, 2005.

[8] L. C. Potter, E. Ertin, J.T. Parker, M. Cetin, "Sparsity and compressed sensing in radar imaging," Proc. IEEE, vol. 98, no. 6, pp. 1006-1020, June 2010.

[9] E. Zastrow, S. K. Davis, M. Lazebnik, F. Kelcz, B. D. Van Veen, S. C. Hagness, Database of 3D grid-based numerical breast phantoms for use in computational electromagnetics simulations.

[10] M. Lazebnik, L. McCartney, D. Popovic, C. B. Watkins, M. J. Lindstrom, J. Harter, S. Sewall, A. Magliocco, J. H. Booske, M. Okoniewski, and S. C. Hagness, "A large-scale study of the ultrawideband microwave dielectric properties of normal breast tissue obtained from reduction surgeries," Physics in Medicine and Biology, vol. 52, pp. 2637-2656, April 2007.

[11] M. Nikolic, J. Dinkic, N. Milosevic, and B. Kolundzija, "Sparse localization of tumors inside an inhomogeneous breast," International Conference on Electromagnetics in Advanced Applications (ICEAA), 2015, vol., no., pp.1056-1059, 7-11 Sept. 2015.

[12] W.C. Chew, Waves and fields in inhomogenousmedia, Wiley-IEEE Press, February 1999.

[13] P. C. Hansen and D. P. O'Leary, "The use of the L-curve in the regularization of discrete ill-posed problems," *SIAM J. Sci. Comput.*, vol. 14, no. 6, pp. 1487–1503, 1993.

[14] N. Milosevic, M. Nikolic, B. Kolundzija, J. Music, "Numerical Heterogeneous Breast Phantoms with Different Resolutions," EUCAP 2015, Lisbon, Portugal.

[15] http://www.wipl-d.com/.